Nucleation versus instability race in strained films

Kailang Liu, Isabelle Berbezier,[*] Thomas David, Luc Favre, Antoine Ronda, and Marco Abbarchi

Institut Matériaux Microélectronique Nanoscience de Provence, Aix-Marseille Université, UMR CNRS 6242, 13997 Marseille, France

Peter Voorhees

Department of Materials Science and Engineering, Northwestern University, Evanston, Illinois 60208-3108, USA

Jean-Noël Aqua[†]

Institut des Nanosciences de Paris, Université Pierre et Marie Curie Paris 6 and CNRS UMR 7588, 4 place Jussieu, 75252 Paris, France

Under the generic term "Stranski-Krastanov" are grouped two different growth mechanisms of SiGe quantum dots. They result from the self-organized Asaro-Tiller-Grinfel'd (ATG) instability at low strain, while at high strain, from a stochastic nucleation. While these regimes are well known, we elucidate here the origin of the transition between these two pathways thanks to a joint theoretical and experimental work. Nucleation is described within the master equation framework. By comparing the time scales for ATG instability development and three-dimensional (3D) nucleation onset, we demonstrate that the transition between these two regimes is simply explained by the crossover between their divergent evolutions. Nucleation exhibits a strong exponential deviation at low strain while ATG behaves only algebraically. The associated time scale varies with $\exp(1/x^4)$ for nucleation, while it only behaves as $1/x^8$ for the ATG instability. Consequently, at high (low) strain, nucleation (instability) occurs faster and inhibits the alternate evolution. It is then this different kinetic evolution which explains the transition from one regime to the other. Such a kinetic view of the transition between these two 3D growth regimes was not provided before. The crossover between nucleation and ATG instability is found to occur both experimentally and theoretically at a Ge composition around 50% in the experimental conditions used here. Varying the experimental conditions and/or the system parameters does not allow us to suppress the transition. This means that the SiGe quantum dots always grow via ATG instability at low strain and nucleation at high strain. This result is important for the self-organization of quantum dots.

I. INTRODUCTION

Quantum dots (QDs) are nowadays extensively grown by different techniques and used in a broad range of applications, from high-performance broadband photodiodes [1] to quantum information processing [2], quantum cryptography with photon quantum bits [3,4], light emitting diodes with photonic QD crystals in microcavity [5], QD transistors [6], QD solar cells [7,8], etc. Many efforts have been devoted to circumvent the low quantum efficiency of Si and Ge QDs associated with an indirect band gap issue. Band folding in strained heterostructures was expected to create quasidirect band structure [9–11] and to increase radiative recombination [12]. Various configurations of self-assembled Si/Ge multiple quantum dots [13], nanopatterned microdisks [10], and nanopatterned superlattices pyramidal QDs [14] have been elaborated to adjust the band structure.

Complex design of QD devices allows us to mix different signals such as spins and carriers or photons and carriers with a large variety of QDs per chip with multiple functions, whose placement and homogeneity commonly request a combination of nanotechnology and self-organization steps. Devices such as single (or some) electron transistors are also configured with one, two, or three QDs closely packed on laterally confined active areas. Nevertheless, most QD systems fabricated by

nanotechnological tools are limited by their intrinsic lack of homogeneity, which reduces to only a small number of relevant dots to be achieved per chip. At the opposite, MOSFET devices require perfectly flat, Ge-rich, free of defects and fully strained two-dimensional (2D) thin films epitaxially deposited on an ultrasmall transistor gate. Whatever the end-use application, ultimate fabrication of devices necessitates a perfect control of the island formation and evolution behavior over a large range of composition.

Despite the large number of studies dedicated to the SiGe system, an unified quantitative description of the morphological evolution of the epitaxial layers towards QDs formation whatever the experimental conditions are, is still lacking. While the major technological challenge is to engineer reproducible quantum devices based on QDs located at will using self-organization processes allowing QDs control and scalability, we focus here on the morphological transition between SiGe epitaxial layers and QDs.

Since the QDs growth significantly differs in rather similar experiments and is a matter of confusion or controversy, we give here quantitative insights on the very first steps of the out-of-equilibrium evolution from bidimensional layer to QDs and we clarify the transition pathway from the ATG instability regime to the 3D nucleation regime which was not elucidated so far. We develop here a kinetic model to rationalize the competition between the two 3D growth modes: ATG instability and islands nucleation and to evaluate the crossover concentration x_c that separates them. It incorporates the main ingredients that rule island growth, i.e., the driving

_____

[*]isabelle.berbezier@im2np.fr
[†]aqua@insp.jussieu.fr

elasticity vs the inhibiting capillarity, and neglects other details such as reconstruction, alloying, surface stress, or inhomogeneities [15]. We derive an analytic expression for island nucleation barrier that is found to noticeably depend on the amount of strain, i.e., on x. The associated nucleation time scale exponentially depends on $\exp(1/x^4)$, while the ATG-instability time scale only displays an algebraic dependence on $1/x^8$. As a result, we find a clear crossover between these two time scales at a critical value $x_c \simeq 0.5$ in SiGe systems. This value is confirmed by experiments especially dedicated to investigate this crossover. This study provides a deep understanding of the formation, evolution, and self-organization of QDs.

II. EXPERIMENTAL RESULTS

The experiments to identify the two different evolution pathways are performed in a Riber MBE (molecular-beam epitaxy) system with pressure down to 10^{-11} Torr. The Si deposition flux is produced by electron-beam evaporation while the Ge flux comes from an effusion cell. The deposition rates are both precisely calibrated by reflection high-energy electron diffraction. The Si(001) substrate is first cleaned by chemical methods and then transferred into the MBE growth chamber. After flashing the substrate at $1000\,°C$ for 3 min, a buffer layer with a thickness of 40 nm is deposited to make a reproducible clean surface at $750\,°C$. Then, the substrate temperature is decreased to $550\,°C$, Si and Ge are co-deposited with SiGe rate of 0.04–0.05 nm s^{-1}. The sample holder is always kept rotating during the deposition. As deposition stops, the samples are immediately cooled down and subsequently taken out for morphological characterization using atomic force microscopy in noncontact mode. We precisely control the epilayer thickness to catch the onset of surface
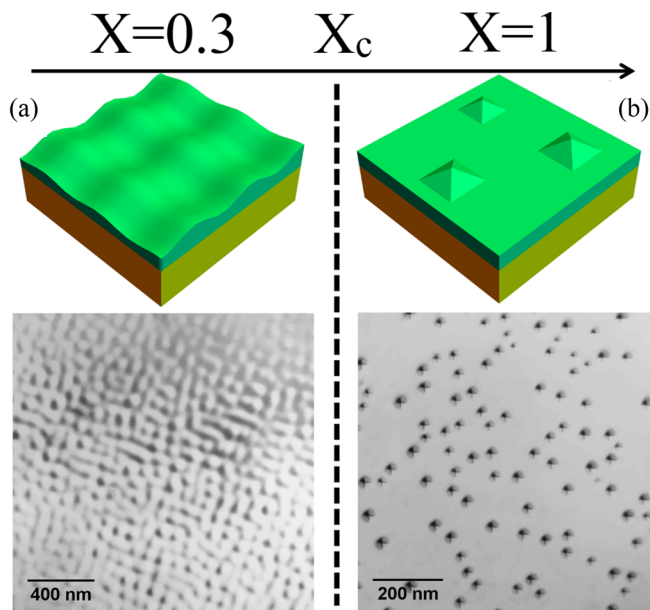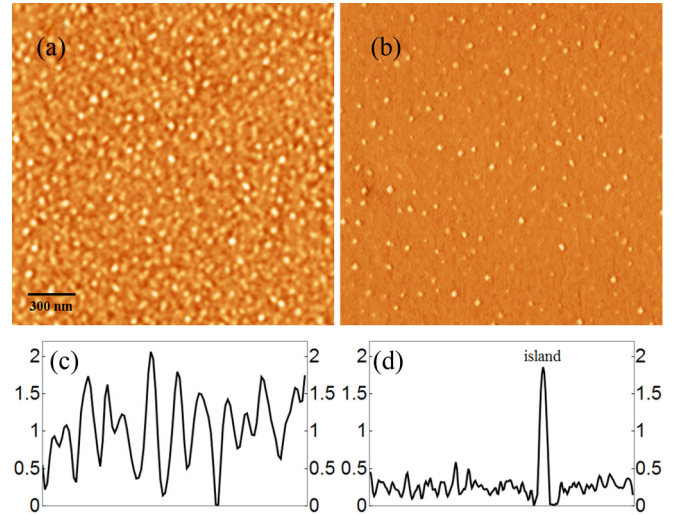
FIG. 2. AFM images of (a) 2 nm $Si_{0.5}Ge_{0.5}$ and (b) 1.3 nm $Si_{0.4}Ge_{0.6}$ films deposited on Si(001). The image sizes are $2\mu m \times 2\mu m$ and their vertical scale is 7 nm. Images (c) and (d) are lines profiles corresponding respectively to (a) and (b).

roughening and hence the first steps of the morphological evolution. In $Si_{1-x}Ge_x$ films on Si, one can taylor the amount of strain by varying the mean Ge concentration x. At low x, see Fig. 1, one finds an instability in connection with self-organized phenomena where dynamics builds long-range structures [16,17]. This instability, which begins by a small unfacetted corrugation, is nucleationless [18,19] and leads after some coarsening to facetted QDs [20]. At high x conversely, see Fig. 1, the first stages of nucleation already involve facetted dots [21] that nucleate randomly without any long-range order [22,23].

The two typical evolution pathways are clearly visible in Fig. 2 for a 2-nm-thick $Si_{0.5}Ge_{0.5}$ film and for a 1.3-nm-thick $Si_{0.4}Ge_{0.6}$ film. In Fig. 2(a) the morphology roughens on the whole surface as described by the ATG instability [18,19]. The wavelength of this corrugation is conveniently extracted from a ringlike Fourier transform image, in good agreement with the experimental results for this instability [18]. The continuous roughening is more clearly highlighted in a typical line profile in Fig. 2(c). On the contrary, for the $Si_{0.4}Ge_{0.6}$ film in Fig. 2(b), islands nucleate discretely on the surface while the rest of the surface remains flat. This is evidenced by the profile in Fig. 2(d) that exhibits isolated islands separated by a wetting layer in which roughness is around 0.3 nm, merely in the magnitude of AFM noise. Its Fourier transform image is a full disk, showing no long-range order. As a consequence, we conclude that the crossover concentration between the nucleation and instability growth mode lies around 0.55 ± 0.05 at $550\,°C$.

III. THEORETICAL RESULTS

A. Nucleation theory

To characterize the nucleation process, we consider the classical theory of nucleation [24] which is adequate given the large critical sizes (a few hundreds of atoms) found in experiments [21]. We first compute the energy barrier

FIG. 1. Graphical representation and TEM plane view images of the two growth modes at work in SiGe strained films: (a) at low strain for a typical $Si_{0.7}Ge_{0.3}$ film on Si(001) and (b) at high strain for a typical Ge film on Si(001).

associated with the formation of quantum dots from a flat film [25–30] in the regime of homogeneous nucleation. Heterogeneous nucleation, e.g., nucleation at step edges or surface vacancies [31], which is not expected to occur due to the very large critical size, is not considered. A similar assumption has already been put forward in most nucleation models involving SiGe QDs. We consider that the islands have a square-base pyramidal shape with (105) facets that corresponds to the first well-defined hut clusters shape found in experiments after the initial prepyramid embryo [21,32] and we compute all the barriers analytically. The effect of the islands initial shapes is discussed in the Appendix.

The total energy results from the competition between elasticity and capillarity. The formation energy of the pyramid (the difference in energy between one pyramid of volume V on top of a wetting layer of thickness h_w, and one flat layer of thickness h_0) is made of the well-known main contributions [33]

$$\Delta E = \Delta E^{\text{surf}} + \Delta E^{\text{ed}} + \Delta E^{\text{el}}, \qquad (1)$$

with the surface energy contribution ΔE^{surf}, edge energy ΔE^{ed}, and elastic relaxation of the misfit strain ΔE^{el}. Mass conservation enforces the balance $h_w = h_0 - \rho V/a$ where a is the lattice parameter ($a = 0.27$ nm in SiGe) and $1/\rho$ is the surface available for each island.

The surface energies of the (001) and (105) facets, $\gamma^{(001)}$ and $\gamma^{(105)}$, depend on different parameters such as the film thickness, composition, etc. The surface composition of a SiGe film deposited on Si is still a matter of experimental investigation. One knows that Ge segregates so that the surface is enriched in Ge [34]. As a simplification, we consider the limiting case of a surface composition $x^s = 1$. It corresponds to experimental results that indicate a full enrichment of the surface in Ge even in deposited alloys [35]. Moreover, we consider films above their Stranski-Krastanov critical thickness so that wetting interactions do not enter significantly in the energy barrier. For a pyramid with facet angle θ, volume V, and base length $L = \alpha V^{1/3}$ [with $\alpha = (6/\tan\theta)^{1/3}$], see Fig. 3, one finds

$$\Delta E^{\text{surf}} = \gamma_{\text{Ge}}^{(001)} \eta L^2, \qquad (2)$$

with the capillary number

$$\eta = \frac{\gamma_{\text{Ge}}^{(105)}}{\gamma_{\text{Ge}}^{(001)}} \frac{1}{\cos\theta} - 1 \qquad (3)$$

that describes the stability of the (001) surface with respect to faceting to (105). When $\eta > 0$, the creation of a (105) facet is overall a cost in energy, so that capillarity is a resistant force [36,37] We consider in the following $\gamma_{\text{Ge}}^{(001)} = 60.5$ meV Å^{-2}, see Refs. [38,39], while $\gamma_{\text{Ge}}^{(105)}$ is given by η as discussed below. Finally, we also include an edge energy σ^{ed} [25,28,40] to describe the pyramidal shape with a mean value for the pyramid and pyramid/wetting layer angles, so that

$$\Delta E^{\text{ed}} = \frac{4H}{\tan\theta}(2 + \sqrt{2 + \tan^2\theta})\,\sigma^{\text{ed}}. \qquad (4)$$

As regards elasticity, mechanical equilibrium equations may be solved exactly in the systems under investigation that display small slopes [at most $11°$ for the (105) facets]. In the small slope approximation, a film with a free surface $z = h(\mathbf{r})$
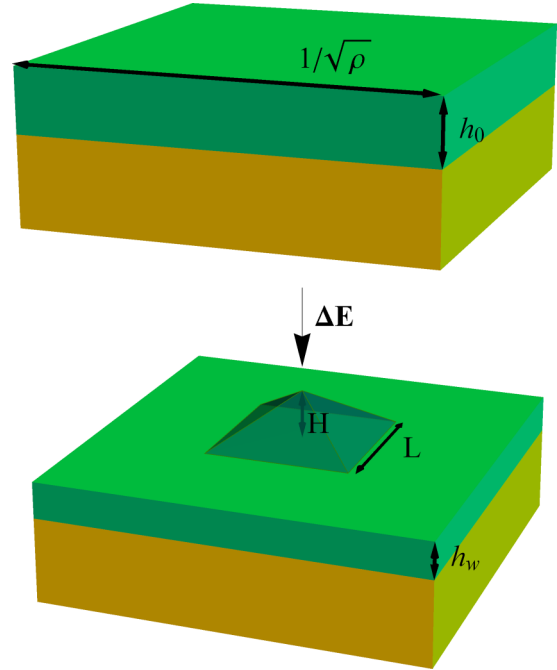
FIG. 3. Geometry of the system, where each island with a square-base pyramidal geometry, grows on a zone of area $1/\rho$ on top of a wetting layer of thickness h_w.

has an elastic energy [41]

$$\mathcal{E}^{\text{el}} = \mathcal{E}_0 \int d\mathbf{r}\{h(\mathbf{r}) - \zeta h(\mathbf{r})\mathcal{H}_{ii}[h(\mathbf{r})]\}, \qquad (5)$$

with the energy density $\mathcal{E}_0 = Y_f m^2/(1 - \nu_f)$ and coefficient $\zeta = Y_f(1 - \nu_s^2)/Y_s(1 - \nu_f)$, where Y and ν are the Young's modulus and Poisson's ratio while subscripts f and s refer to the film and substrate. The elastic contribution to the nucleation barrier can be computed exactly [42], with the result

$$\Delta E^{\text{el}} = -\zeta\, p\, \mathcal{E}_0\, V, \qquad (6)$$

for a square base pyramid, with

$$p = 4(\sqrt{2} - 1)[1 + \ln(1 + \sqrt{2})]\tan\theta/\pi. \qquad (7)$$

As a whole, the energy barrier ΔE reduces to the typical form $\Delta E = \tilde{\sigma} v^{1/3} + \tilde{\gamma} v^{2/3} - \tilde{p} v$, with $\tilde{\sigma} = 2(2 + \sqrt{2 + \tan^2\theta})\sigma^{\text{ed}}$, $\tilde{\gamma} = \gamma_{\text{Ge}}^{(001)}\eta$, $\tilde{p} = \zeta\, p\, \mathcal{E}_0 \tan\theta/6$, and $v = 6V/\tan\theta$. Its typical variation is plotted in Fig. 4 and shows the existence of an energy barrier ΔE^*,

$$\Delta E^* = \frac{1}{27\tilde{p}^2}[\tilde{\gamma}(2\,\tilde{\gamma}^2 + 9\,\tilde{p}\,\tilde{\sigma}) + 2(\tilde{\gamma}^2 + 3\,\tilde{p}\,\tilde{\sigma})^{3/2}], \quad (8)$$

at a critical volume V^* such as $V^{*\,1/3} = (\tilde{\gamma} + \sqrt{\tilde{\gamma}^2 + 3\tilde{\sigma}\,\tilde{p}})/3\tilde{p}$.

With this nucleation barrier, one can derive the nucleation theory based on the master equation [24,43]

$$\frac{d\rho_n}{dt} = \sum_m [f_{m,n}\,\rho_m - f_{n,m}\,\rho_n] \qquad (9)$$

that relates the densities ρ_n of clusters with n atoms, with the frequencies $f_{m,n}$ of the transitions from m to n-atom clusters.
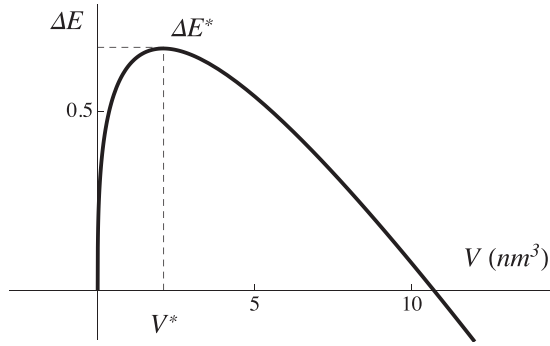
FIG. 4. Nucleation barrier ΔE as a function of the pyramid volume V with the parameters described below.

When only one-atom events occur, only the frequencies $f_n = f_{n,n+1}$ matter. They may be estimated as

$$f_n = \gamma_n \alpha D_s \rho_1, \qquad (10)$$

with the attachment coefficient γ_n, capture coefficient α, adatom density $\rho_1(t)$, and surface diffusion coefficient $D_s(T)$. In the following, we will use $\alpha \simeq 1$, $\gamma_n \simeq 1$, $D_s = a^2 \nu_0 e^{-\beta E_{\text{diff}}}$ with $\nu_0 \simeq 10^{13}$ s^{-1} and the diffusion barrier $E_{\text{diff}} = 0.83$ eV in Si [44]. We also make the approximation $\rho_1 = \frac{1}{a^2} e^{-\beta E_2}$ with the attachment energy $E_2 \simeq 0.3$ eV [27]. The master equation has a stationary solution characterized by a flux of nucleation per unit time and surface [24,43]

$$J^{\text{st}} = Z f_{n^*} \rho_{n^*}, \qquad (11)$$

with f_{n^*} as the growth frequency of a critical cluster with n^* atoms (corresponding to the critical volume V^*), and the critical cluster density

$$\rho_{n^*} = \rho_1 e^{-\beta \Delta E^*}. \qquad (12)$$

In (11), the Zeldovich factor is given by [24,43]

$$Z = \sqrt{-\frac{\partial^2 \Delta E}{\partial n^2}\bigg|_{n^*} \frac{1}{2\pi k_B T}} \qquad (13)$$

that reduces here to

$$Z = \frac{2a^3 \sqrt{\beta}}{\tan\theta \sqrt{\pi} \tilde{\sigma}^2} (\tilde{\gamma} - \sqrt{\tilde{\gamma}^2 + 3\tilde{\sigma}\, \tilde{p}})(\tilde{\gamma}^2 + 3\tilde{\sigma}\, \tilde{p})^{1/4}. \quad (14)$$

The flux J^{st} is associated with the typical time scale for nucleation

$$\tau^{\text{nuc}} = \frac{1}{J^{\text{st}} \lambda^2}, \qquad (15)$$

where we choose to consider nucleation over the typical island zone λ^2 defined by the experimental density $\lambda = 1/\sqrt{\rho}$, with $\rho \simeq 10^{13}$ m^{-2}.

B. Asaro-Tiller-Grinfel'd instability

With this time scale in hand, we turn to the ATG morphological instability [45,46]. It may be captured by the continuum description of surface diffusion governed by $\partial h/\partial t = D \Delta_s \mu$ with the diffusion coefficient D, surface Laplacian Δ_s and chemical potential μ [44]. The latter includes the capillary term

$\gamma \Delta_s h$ and the elastic energy density $\mathcal{E}_0$ so that dimensional analysis leads to the instability space and time scales [47]

$$l_{\text{ATG}} = \frac{\gamma_f}{2\zeta \mathcal{E}_0} \quad \text{and} \quad t^{\text{ATG}} = \frac{l_{\text{ATG}}^4}{D \gamma_f}, \qquad (16)$$

with the surface energy $\gamma_f = \gamma_{\text{Ge}}^{(001)}$ and the elastic energy density given above that is proportional to $m^2 = (0.042\, x)^2$. Hence, t^{ATG} is proportional to $1/x^8$ [48].

IV. COMPARISON BETWEEN THE INSTABILITY AND NUCLEATION TIME SCALES

We plot in Fig. 5 the typical time scales of nucleation and of the ATG instability. The nucleation time τ^{nuc} displays a strong exponential increase at low x, overshooting the rather slow varying t^{ATG}. Hence, we argue that the two pathways (instability vs nucleation) are dictated by kinetics: for large enough x, $\tau^{\text{nuc}} \ll t^{\text{ATG}}$ so that nucleation occurs first, relaxes partially the elastic strain, and prevents the occurrence of the ATG instability. On the contrary, for low enough x, $\tau^{\text{nuc}} \gg t^{\text{ATG}}$ and only the instability has time to occur. The crossover between the two time scales may be rationalized by the strong decrease in the critical clusters density ρ_{n^*} when x decreases. Indeed, when x decreases, the surface energy contribution is constant while the amplitude of the elastic relaxation decreases as $\mathcal{E}_0 \propto x^2$ so that ΔE^*, the maximum for ΔE, increases. Because this energy barrier enters in a Boltzmann factor in ρ_{n^*}, the nucleation rate exponentially decreases with x. To quantify this effect, one may simplify the expression of J^{st} by performing a small-x expansion of ΔE^*, with the result

$$\tau^{\text{nuc}} \approx \tau_0^{\text{nuc}} \exp\left[\beta\left(b\frac{\gamma^3}{x^4} + c\frac{\gamma \sigma^{\text{ed}}}{x^2}\right)\right], \qquad (17)$$

with some constants τ_0^{nuc}, b, and c. This approximation is shown in Fig. 5 and does indeed match the exact result at low x. With this approximation, it is clear that the capillary vs elasticity balance leads to a strong $\exp(1/x^4)$ divergence of τ^{nuc} at low x that quickly overshoots the ATG time scale that "only" behaves as $1/x^8$. The system under study may include
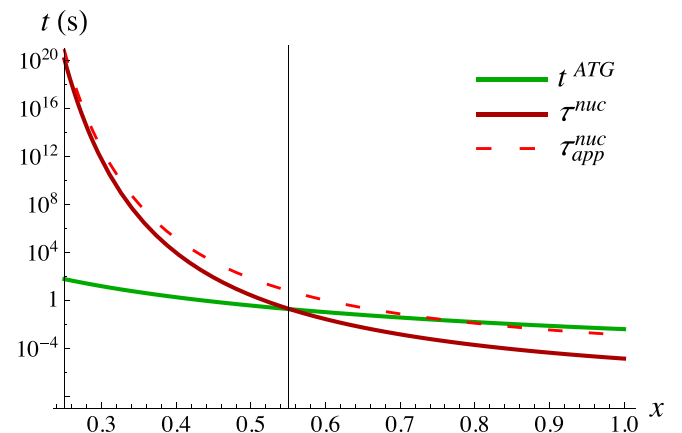
FIG. 5. Typical time scales for nucleation τ^{nuc} (red–dark gray line) and ATG instability t^{ATG} (green–light gray line) as a function of the film Ge composition x for $\eta = 0.003$ and $\sigma^{\text{ed}} = 3.3$ meV Å^{-1}. The red dotted line corresponds to the analytic approximation (17).

extra effects such as alloying (intermixing, segregation, surface inhomogeneities), surface reconstruction inhomogeneity and evolution, wetting effects, surface stress, inhomogeneous nucleation, etc. However, we argue that the main scenario ruling the crossover between the ATG instability and nucleation is contained in this scenario: when x decreases, the elastic driving force decreases, the energy barrier increases so that nucleation occurs over an exponentially divergent time scale.

The data in Fig. 5 are computed with parameters typical of SiGe systems as described above [49]. The intersection between the two time scales occurs around $x_c \simeq 0.55$ that is consistent with the experimental results. This value depends on the physical parameters (see the Appendix). The classical nucleation theory includes different parameters that are approximate (capture zone, etc.) but which precise values are not relevant for the existence of the crossover and do not affect its composition value. The two parameters that prove to be quantitatively important for x_c are the capillary number η and edge energy σ^{ed}. We consider here a positive but small capillary number $\eta = 0.003$ that corresponds to $\gamma_{\mathrm{Ge}}^{(105)} = 59.5$ meV Å^{-2}, only 1 meV lower than $\gamma_{\mathrm{Ge}}^{(001)}$. This value leads to a crossover x_c in the vicinity of 0.55 for $\sigma^{\mathrm{ed}} = 3.3$ meV Å^{-1}. The latter edge energy is chosen accordingly to the atomistic estimation in Ref. [50] that is 10 meV Å^{-1}. Given the uncertainties on the physical parameters that have already been discussed in many previous models, the comparison between theory and experiment is valid. To go further, we characterize the dependence of the model with the more crucial parameters η and σ^{ed}. For more details see the Appendix. We conclude from this analysis that even when considering variations of these parameters, the crossover remains expected around $x_c < 0.5$.

V. CONCLUSION

We performed a joint experimental and theoretical work to rationalize the competition between two growth modes in strained films: the nucleation of islands and the ATG morphological instability that both eventually lead to quantum dots. We show experimentally in SiGe systems that the instability occurs for a Ge concentration $x \lesssim 0.5$ while quantum dots stochastically nucleate at $x \gtrsim 0.5$. We computed the nucleation barrier and time scale τ^{nuc} from rate theory. We show that τ^{nuc} diverges exponentially at low x, with a Boltzmann factor $\exp[\alpha/k_B T x^4]$ while the instability time scale evolves only as $1/x^8$. These divergent evolutions explain why 3D nucleation occurs faster at large strain since its time scale is shorter, while it is frozen at low strain, allowing

time for the ATG instability to occur. Consequently, although thermodynamic phenomena were put forward in most previous models, we demonstrate in this work that the transition between ATG instability and 3D nucleation regimes is ruled by kinetics.

APPENDIX: EVOLUTION OF THE TRANSITION'S CRITICAL COMPOSITION

While nucleation is a stochastic phenomenon and instability is self-organized, it is an important issue to determine whether one could modify or even suppress the transition between ATG instability and nucleation in order to better self-organize Ge rich islands (using ATG instability). In this context, we examined the effect of variations of the system parameters on the transition. The two main parameters that can modify the transition are η and σ^{ed}. If we consider a mean value of $\eta = 0.003$, and we change σ^{ed} between 3 and 4 meV Å^{-1}, one finds $x_c = 0.50$ and 0.71, respectively. Also, considering a mean value of $\sigma^{\mathrm{ed}} = 3.3$ meV Å^{-1}, if we vary η between 0.0046 and 0.0013 (that corresponds to $\gamma_{\mathrm{Ge}}^{(001)} = 59.4$ and 59.6 meV Å^{-2}), one finds $x_c = 0.73$ and 0.37.

The growth temperature could also affect the crossover composition. If we change the temperature to $T = 650\,^{\circ}$C, we get $x_c \simeq 0.48$. At higher temperatures, intermixing is supposed to play a significant role [20] and will decrease the elastic driving force. Lastly, the surface composition could also be important. By changing x_s to 0.9, we find $x_c = 0.8$ using a Vegard's law for the surface energy with $\gamma_{\mathrm{Si}} = 90$ meV Å^{-2} both for (001) and (105) orientations [38,39]—note that in this case η changes significantly to 0.0053. The shape of the islands could also affect the transition. We then determined the effect of the shapes of the nucleating islands by considering for example truncated pyramids that have also been found experimentally. We computed numerically the elastic energy for a pyramid truncated at half height, and we found typically an increase in ΔE^* of 0.1 eV. As a conclusion, considering variations of the main parameters as a function of the experimental conditions (surface concentration, reconstruction, alloying, etc.), first validates the overall scenario with a crossover expected to be around 0.5 and second shows the impossibility to suppress the transition between ATG instability and nucleation. It is then not possible to use ATG instability to self-organize Ge rich islands.

[1] J. Michel, J. Liu, and L. C. Kimerling, Nat. Photon. **4**, 527 (2010).

[2] G. Juska, V. Dimastrodonato, L. O. Mereni, A. Gocalinska, and E. Pelucchi, Nat. Photon. **7**, 527 (2013).

[3] J. L. O'Brien, G. J. Pryde, A. G. White, T. C. Ralph, and D. Branning, Nature (London) **426**, 264 (2003).

[4] M. Bayer, P. Hawrylak, K. Hinzer, S. Fafard, M. Korkusinski, Z. Wasilewski, O. Stern, and A. Forchel, Science **291**, 451 (2001).

[5] J. Xia, Y. Ikegami, Y. Shiraki, N. Usami, and Y. Nakata, Appl. Phys. Lett. **89**, 201102 (2006).

[6] C. Biasotto, L. Nanver, J. Moers, J. Gerharz, G. Mussler, J. van der Cingel, J. Zhang, G. Bauer, O. Schmidt, and L. Miglio, IEEE Electron Device Lett. **31**, 1083 (2010).

[7] T. Tayagaki, Y. Hoshi, and N. Usami, Sci. Rep. **3**, 2703 (2013).

[8] A. Luque and A. Martí, Phys. Rev. Lett. **78**, 5014 (1997).

[9] T. Zabel, N. Sircar, N. Hauke, J. Zweck, M. Döblinger, M. Kaniber, J. J. Finley, G. Abstreiter, Y. Arakawa, and D. Bougeard, Appl. Phys. Lett. **103**, 063105 (2013).

[10] R. Chen, S. Gupta, Y.-C. Huang, Y. Huo, C. W. Rudy, E. Sanchez, Y. Kim, T. I. Kamins, K. C. Saraswat, and J. S. Harris, Nano Lett. **14**, 37 (2013).

[11] J. R. Jain, A. Hryciw, T. M. Baer, D. A. Miller, M. L. Brongersma, and R. T. Howe, Nat. Photon. **6**, 398 (2012).

[12] E. Barbagiovanni, D. Lockwood, N. Rowell, R. Costa Filho, I. Berbezier, G. Amiard, L. Favre, A. Ronda, M. Faustini, and D. Grosso, J. Appl. Phys. **115**, 044311 (2014).

[13] A. I. Yakimov, V. V. Kirienko, V. A. Armbrister, A. A. Bloshkin, and A. V. Dvurechenskii, Phys. Rev. B **90**, 035430 (2014).

[14] S. R. C. Pinto, M. Buljan, A. Chahboun, M. A. Roldan, S. Bernstorff, M. Varela, S. Pennycook, N. P. Barradas, E. Alves, S. I. Molina, M. M. D. Ramos, and M. J. M. Gomes, J. Appl. Phys. **111**, 074316 (2012).

[15] J. Villain, J. Cryst. Growth **275**, e2307 (2005).

[16] A. J. Pidduck, D. J. Robbins, A. G. Cullis, W. Y. Leong, and A. M. Pitt, Thin Solid Films **222**, 78 (1992).

[17] I. Berbezier, B. Gallas, A. Ronda, and J. Derrien, Surf. Sci. **412-413**, 415 (1998).

[18] P. Sutter and M. G. Lagally, Phys. Rev. Lett. **84**, 4637 (2000).

[19] R. M. Tromp, F. M. Ross, and M. C. Reuter, Phys. Rev. Lett. **84**, 4641 (2000).

[20] J.-N. Aqua, I. Berbezier, L. Favre, T. Frisch, and A. Ronda, Phys. Rep. **522**, 59 (2013).

[21] B. Voigtänder, Surf. Sci. Rep. **43**, 127 (2001).

[22] D. J. Eaglesham and M. Cerullo, Phys. Rev. Lett. **64**, 1943 (1990).

[23] Y. W. Mo, D. E. Savage, B. S. Swartzentruber, and M. G. Lagally, Phys. Rev. Lett. **65**, 1020 (1990).

[24] D. Kashchiev, *Nucleation, Basic Theory with Application* (Butterworth-Heinemann, London, 2000).

[25] V. A. Shchukin, N. N. Ledentsov, P. S. Kop'ev, and D. Bimberg, Phys. Rev. Lett. **75**, 2968 (1995).

[26] P. Müller and R. Kern, Appl. Surf. Sci. **102**, 6 (1996).

[27] M. R. McKay, J. A. Venables, and J. Drucker, Phys. Rev. Lett. **101**, 216104 (2008).

[28] M. Brehm, F. Montalenti, M. Grydlik, G. Vastola, H. Lichtenberger, N. Hrauda, M. J. Beck, T. Fromherz, F. Schäffler, L. Miglio, and G. Bauer, Phys. Rev. B **80**, 205321 (2009).

[29] B. J. Spencer and J. Tersoff, Phys. Rev. B **87**, 161301 (2013).

[30] X. L. Li, C. X. Wang, and G. W. Yang, Progress Mater. Sci. **64**, 121 (2014).

[31] F. F. Liu, F. Wu, and M. G. Lagally, Chem. Rev. **97**, 1045 (1997).

[32] A. Vailionis, B. Cho, G. Glass, P. Desjardins, D. G. Cahill, and J. E. Greene, Phys. Rev. Lett. **85**, 3672 (2000); P. D. Szkutnik, A. Sgarlata, S. Nufris, N. Motta, and A. Balzarotti, Phys. Rev. B **69**, 201309 (2004).

[33] J. Tersoff, B. J. Spencer, A. Rastelli, and H. von Känel, Phys. Rev. Lett. **89**, 196104 (2002).

[34] K. Nakagawa and M. Miyao, J. Appl. Phys. **69**, 3058 (1991); F. Liu and M. G. Lagally, Phys. Rev. Lett. **76**, 3156 (1996); B. Voigtländer and M. Kästner, Phys. Rev. B **60**, R5121(R) (1999); G. Capellini, M. De Seta, and F. Evangelisti, Appl. Phys. Lett. **78**, 303 (2001); M. S. Leite, J. L. Gray, R. Hull, J. A. Floro, R. Magalhães-Paniago, and G. Medeiros-Ribeiro, Phys. Rev. B **73**, 121308(R) (2006); M. Brehm, M. Grydlik, H. Lichtenberger, T. Fromherz, N. Hrauda, W. Jantsch, F. Schäffler, and G. Bauer, Appl. Phys. Lett. **93**, 121901 (2008).

[35] A. Portavoce, F. Bassani, A. Ronda, and I. Berbezier, Surf. Sci. **519**, 185 (2002); I. Berbezier, M. Descoins, B. Ismail, H. Maaref, and A. Ronda, J. Appl. Phys. **98**, 063517 (2005).

[36] I. Daruka, C. Grossauer, G. Springholz, and J. Tersoff, Phys. Rev. B **89**, 235427 (2014).

[37] Contrarily, $\eta < 0$ would describe a system where the creation of (105) is a driving force. It was put forward to rationalize the existence of nanowires in subcritical systems (see Ref. [51]), but entropic effects, reconstruction coexistence, and composition inhomogeneities enforce a high level of uncertainty.

[38] G.-H. Lu and F. Liu, Phys. Rev. Lett. **94**, 176103 (2005).

[39] D. Scopece, F. Montalenti, and M. J. Beck, Phys. Rev. B **85**, 085312 (2012).

[40] K. A. Lozovoy, A. P. Kokhanenko, and A. V. Voitsekhovskii, Cryst. Growth Design **15**, 1055 (2015).

[41] J.-N. Aqua and T. Frisch, Phys. Rev. B **82**, 085322 (2010).

[42] C. Duport, C. Priester, and J. Villain, *Equilibrium Shape of a Coherent Epitaxial Cluster* (World Scientific, Singapore, 1997), p. 73.

[43] L. Ratke and P. W. Voorhees, *Growth and Coarsening* (Springer, Berlin, 2010).

[44] B. J. Spencer, P. W. Voorhees, and S. H. Davis, Phys. Rev. Lett. **67**, 3696 (1991).

[45] R. J. Asaro and W. A. Tiller, Metal. Trans. **3**, 1789 (1972).

[46] M. A. Grinfeld, Sov. Phys. Doklady **31**, 831 (1986).

[47] J.-N. Aqua, A. Gouyé, A. Ronda, T. Frisch, and I. Berbezier, Phys. Rev. Lett. **110**, 096101 (2013); J.-N. Aqua, A. Gouyé, T. Auphan, T. Frisch, A. Ronda, and I. Berbezier, Appl. Phys. Lett. **98**, 161909 (2011).

[48] We use in the following $D = \beta D_0 c \Omega$, with the vacancy surface concentration $c \simeq 1/a^2$, $\Omega = a^3$, and $D_0 = 8.45 \times 10^{-10} e^{-\beta E_d} \mathrm{m^2\,s^{-1}}$ with $E_d = 0.83 \mathrm{eV}$ [44].

[49] As regards elasticity, $\nu^{\mathrm{Si}} = 0.279$, $\nu^{\mathrm{Ge}} = 0.273$, $Y^{\mathrm{Si}} = 1.3 \times 10^{11} \mathrm{J\,m^{-3}}$, $Y^{\mathrm{Ge}} = 1.03 \times 10^{11} \mathrm{J\,m^{-3}}$, $a = 0.27$ nm.

[50] C. M. Retford, M. Asta, M. J. Miksis, P. W. Voorhees, and E. B. Webb, Phys. Rev. B **75**, 075311 (2007).

[51] G. Chen, B. Sanduijav, D. Matei, G. Springholz, D. Scopece, M. J. Beck, F. Montalenti, and L. Miglio, Phys. Rev. Lett. **108**, 055503 (2012).